Applied Physics Letters

Spin–orbit torque field-effect transistor (SOTFET): Proposal for a magnetoelectric memory

Cite as: Appl. Phys. Lett. **116**, 242405 (2020); https://doi.org/10.1063/5.0002909
Submitted: 28 January 2020 • Accepted: 31 May 2020 • Published Online: 15 June 2020

Xiang Li, Joseph Casamento, Phillip Dang, et al.

COLLECTIONS

Paper published as part of the special topic on Spin-Orbit Torque (SOT): Materials, Physics, and Devices

View Online Export Citation CrossMark

ARTICLES YOU MAY BE INTERESTED IN

Study of the perpendicular magnetic anisotropy, spin-orbit torque, and Dzyaloshinskii-Moriya interaction in the heavy metal/CoFeB bilayers with $Ir_{22}Mn_{78}$ insertion
Applied Physics Letters **116**, 242407 (2020); https://doi.org/10.1063/5.0006138

Spin-orbit torque driven multi-level switching in He^+ irradiated W-CoFeB-MgO Hall bars with perpendicular anisotropy
Applied Physics Letters **116**, 242401 (2020); https://doi.org/10.1063/5.0010679

Field-free switching of magnetic tunnel junctions driven by spin-orbit torques at sub-ns timescales
Applied Physics Letters **116**, 232406 (2020); https://doi.org/10.1063/5.0011433

Lock-in Amplifiers up to 600 MHz
Zurich Instruments
Watch

© 2020 Author(s).

Applied Physics Letters ARTICLE scitation.org/journal/apl

Spin–orbit torque field-effect transistor (SOTFET): Proposal for a magnetoelectric memory

Cite as: Appl. Phys. Lett. **116**, 242405 (2020); doi: 10.1063/5.0002909
Submitted: 28 January 2020 · Accepted: 31 May 2020 ·
Published Online: 15 June 2020

View Online Export Citation CrossMark

Xiang Li,[1,a)] Joseph Casamento,[2] Phillip Dang,[3] Zexuan Zhang,[1] Olalekan Afuye,[1] Antonio B. Mei,[2] Alyssa B. Apsel,[1] Darrell G. Schlom,[2] Debdeep Jena,[1,2,4] Daniel C. Ralph,[4,5] and Huili Grace Xing[1,2,4]

AFFILIATIONS

[1]School of Electrical and Computer Engineering, Cornell University, Ithaca, New York 14853, USA
[2]Department of Materials Science and Engineering, Cornell University, Ithaca, New York 14853, USA
[3]School of Applied and Engineering Physics, Cornell University, Ithaca, New York 14853, USA
[4]Kavli Institute at Cornell for Nanoscale Science, Ithaca, New York 14853, USA
[5]Department of Physics, Cornell University, Ithaca, New York 14853, USA

[a)]Author to whom correspondence should be addressed: xl633@cornell.edu

ABSTRACT

Spin-based memories are attractive for their non-volatility and high durability but provide modest resistance changes, whereas semiconductor logic transistors are capable of providing large resistance changes, but lack memory function with high durability. The recent availability of multiferroic materials provides an opportunity to directly couple the change in spin states of a magnetic memory to a charge change in a semiconductor transistor. In this work, we propose and analyze the spin–orbit torque field-effect transistor, a device with the potential to significantly boost the energy efficiency of spin-based memories and to simultaneously offer a palette of functionalities.

Published under license by AIP Publishing. https://doi.org/10.1063/5.0002909

The understanding of spin transport in heterostructures[1] led to the realization of magnetic memories based on giant magnetoresistance (GMR)[2–4] and spin-transfer torque (STT).[5–8] Current research aims to make the writing process for magnetic memories more efficient using spin–orbit torques (SOTs).[9,10] STT and SOT magnetic random access memories (MRAMs) offer the virtues of non-volatility, infinite endurance, and good write speeds.[8] Nonetheless, the modest resistance change between the magnetic "0" and "1" states of STT- and SOT-MRAMs necessitates a substantial current to obtain acceptable readout voltages, impairing read energies and speeds.

In contrast, non-magnetic semiconductor field-effect transistors (FETs) achieve several orders of magnitude resistance change in each switching event. The field effect converts a linear change in the gate voltage into an exponential change in the mobile carrier density in the semiconductor and, consequently, modulates its resistance. Thus, a material that can transduce the change in the spin/magnetic state in a SOT structure into the charge of a semiconductor channel could significantly boost the resistance change of a magnetic memory.

This requirement would be met by recently developed magnetoelectric multiferroic (MF) materials, which simultaneously possess magnetic order and ferroelectricity in a manner that these order parameters are coupled due to the magnetoelectric effect.[11–13] Moreover, exchange coupling of spins in a ferromagnetic (FM) layer to the magnetic order of a multiferroic layer across ferromagnet/multiferroic heterointerfaces has been experimentally demonstrated.[14,15]

Inspired by these recent advances in SOT and multiferroic materials, we propose a promising magnetoelectric memory device, the spin–orbit-torque field-effect transistor (SOTFET). This device aims to combine the virtues of magnetic memories with the large resistance change of FETs, providing both memory and logic functionalities. Analysis of the memory aspect indicates that the SOTFET can offer several orders of magnitude increase in the on–off resistance ratio compared to existing magnetic memories, which can potentially lower the operation energy significantly. The potential logic aspect of the SOTFET would also enable circuit architectures for efficient logic or search functions.[16] In this paper, we present the physical operation of the SOTFET along with a device model and will mainly focus on the memory aspect.

Figure 1 shows the structure of a SOTFET. It resembles an ordinary metal-oxide-semiconductor FET (MOSFET), but with a unique gate stack. The SOTFET gate stack comprises three layers (from top to bottom): a spin–orbit (SO) layer, a ferromagnetic (FM) layer, and a multiferroic (MF) layer, adjacent to a semiconductor channel to which source and drain contacts are made.

Published under license by AIP Publishing

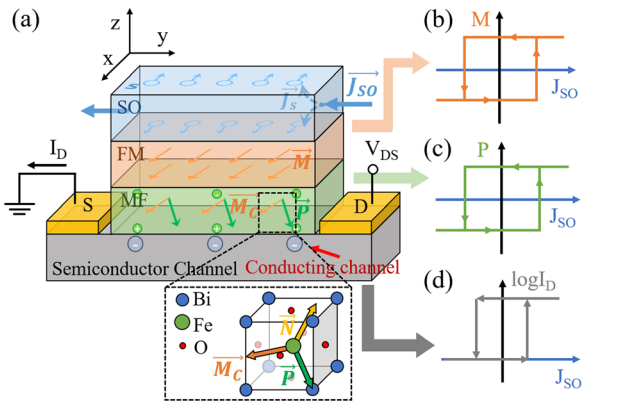

FIG. 1. (a) Device structure and working principle of a SOTFET. A CoFe/$BiFeO_3$ bilayer is employed in this study as the example FM/MF bilayer. **P**, $\mathbf{M}_C$, and **N** in $BiFeO_3$ are indicated in its perovskite unit cell. In equilibrium, **P** points to one of the ⟨111⟩ directions. (b) A charge current J_{SO} through the spin–orbit (SO) layer switches magnetization M in the FM layer, (c) which, in turn, switches polarization P in the MF layer. As a result, (d) the semiconductor channel resistance is modulated and the drain current I_D is used as the readout component.

The working principle of the SOTFET is illustrated in Fig. 1. The state of magnetization **M** of the FM layer is the memory component. When a charge current J_{SO} flows in the SO layer, transverse spin-polarized currents are generated due to spin-momentum locking.[17–22] Spin absorption at the SO/FM interface exerts a spin–orbit torque that switches **M** of the FM,[8,23] as illustrated in Fig. 1(a) and qualitatively plotted in Fig. 1(b). Flowing J_{SO} in the opposite direction switches the magnetization between 1 and 0, identical to the conventional writing mechanism in SOT-MRAMs.

The SOTFET differs from the conventional SOT-MRAMs in the read mechanism. Coupling **M** of the FM with the semiconductor channel would be achieved by the magnetoelectric multiferroic layer. Due to the exchange coupling between the FM and the MF layer,[14,15] the magnetic dipole of the MF layer is also switched with **M** in the FM. Within the MF material, the Dzyaloshinskii–Moriya interaction (DMI)[24,25] effectively couples electric and magnetic dipoles since the weak canted magnetic moment $\mathbf{M}_C$ originates from the DMI.[14,26,27] When $\mathbf{M}_C$ switches polarity, electric polarization **P** in the MF layer deterministically switches in tandem, all in response to J_{SO}, as shown in Fig. 1(c).

The resulting switching of **P** gates the semiconductor channel by shifting the surface potential, similar to the effect in ferroelectric-gate FETs.[28–31] The current I_D flowing in the semiconductor channel is the readout signal, which changes by several orders of magnitude due to the resistance change. Consider the direction of J_{SO} in the SO layer in Fig. 1(a) as writing a 1 in the FM, leading to a high conductivity ON state of the semiconductor. When the current J_{SO} flows in the opposite direction, all the dipoles in the gate stack are flipped. The flipping of **P** then depletes the semiconductor channel, putting it in the OFF state. The resulting transistor output current I_D in response to J_{SO} is shown in Fig. 1(d): it is bi-stable and provides the desired large resistance ratio for efficient readout.

To prove the feasibility of the SOTFET, we quantitatively analyze the dynamical coupling across each interface and the entire device. The analysis to follow shows that the SOTFET behavior is achievable, but requires magnetoelectric multiferroics of specific magnetism and polarization, along with an appropriate hierarchy of strengths for the exchange coupling, DMI, and anisotropy energies within the gate stack.

We choose to build a model based on the most studied heterostructure CoFe/$BiFeO_3$ in this initial modeling effort of SOTFET since the FM/MF heterointerfaces are still poorly understood to date. For a generic FM/MF interface, it is yet difficult to describe the physical phenomena in relatively simple mathematical forms. However, we also note that our results, described in the later sections, show that $BiFeO_3$ is not a suitable multiferroic for SOTFETs because of its strong ferroelectricity and weak magnetism. For a SOTFET, the desired energy hierarchy demands that the suitable multiferroic material should possess a strong magnetic order and a strong exchange coupling with the ferromagnetic material, while its ferroelectric order should deterministically follow the switching of the magnetic order. Bi_2Se_3 is selected as the example SO layer. Other material candidates are discussed in Ref. 32. The aim of this model is to guide experiments by pointing toward desired heterointerface choices.

The magnetization **M** of the FM layer is switched by spin–orbit torque (SOT). For simplicity, we assume single-domain macrospin behavior. The switching dynamics of this process are captured by the Landau–Lifshitz–Gilbert–Slonczewski (LLGS) equation,[6,8,33,34]

$$\frac{d\hat{\mathbf{m}}}{dt} = -\gamma\mu_0\hat{\mathbf{m}} \times \mathbf{H}_{eff} + \alpha\hat{\mathbf{m}} \times \frac{d\hat{\mathbf{m}}}{dt} + \left(\frac{\gamma}{M_S}\right)\vec{\tau}_{SOT}, \tag{1}$$

where $\hat{\mathbf{m}}$ is the normalized magnetization of the FM, $\mathbf{H}_{eff}$ is the effective magnetic field acting on $\hat{\mathbf{m}}$, γ is the electron gyromagnetic ratio, μ_0 is the vacuum permeability, α is the Gilbert damping factor, M_S is the saturation magnetization, and $\vec{\tau}_{SOT} = \vec{\tau}_{AD} + \vec{\tau}_{FL}$ is the spin–orbit torque, the sum of the anti-damping (AD) torque $\vec{\tau}_{AD}$ and field-like (FL) torque $\vec{\tau}_{FL}$, which are given by[8,33]

$$\vec{\tau}_{AD} = \left(\frac{\hbar}{2e}\right)\left(\frac{1}{t}\right)j\theta_{AD}\hat{\mathbf{m}} \times (\hat{\mathbf{m}} \times \hat{\mathbf{m}}_p), \text{ and} \tag{2}$$

$$\vec{\tau}_{FL} = \left(\frac{\hbar}{2e}\right)\left(\frac{1}{t}\right)j\theta_{FL}\hat{\mathbf{m}} \times \hat{\mathbf{m}}_p. \tag{3}$$

Here, $\hbar$ is the reduced Planck constant, e is the electron charge, t is the thickness of ferromagnetic (FM) material, $j = J_{SO}$ is the charge current density in the SO layer, $\theta_{AD(FL)}$ is the spin Hall angle of the anti-damping (AD) or field-like (FL) torque from the SO layer, and $\hat{\mathbf{m}}_p$ is the normalized spin polarization.

The effective field $\mathbf{H}_{eff} = \mathbf{H}_{ext} + \mathbf{H}_a + \mathbf{H}_{demag} + \mathbf{H}_{DMI}$, where $\mathbf{H}_{ext}$ is any external magnetic field and $\mathbf{H}_a$ is the anisotropy field with perpendicular magnetic anisotropy (PMA) calculated by $\mathbf{H}_a = \frac{2K}{\mu_0 M_S} m_z\hat{z} \equiv H_k m_z\hat{z}$,[34] where K is the anisotropy constant. $\mathbf{H}_{demag}$ is the demagnetization field as calculated in the study by Beleggia *et al.*[35] The last term $\mathbf{H}_{DMI}$ is the effective magnetic field arising from the effective DMI, which is discussed further below.

Switching of **M** in the FM switches the electric polarization **P** of the MF layer due to the exchange coupling and DMI. The dynamics of **P** are captured by the Landau–Khalatnikov (LK) equation,[31,36,37]

$$\gamma_{FE}\frac{\partial P_i}{\partial t} = -\frac{\partial F}{\partial P_i}, \tag{4}$$

where γ_{FE} is the viscosity coefficient and $P_i (i = x, y, z)$ is the $x/y/z$ component of **P**. F is the total ferroelectric free energy,[37,38]

Published under license by AIP Publishing

$$F(\mathbf{P},\mathbf{u}) = \alpha_1(P_x^2+P_y^2+P_z^2)+\alpha_{11}(P_x^4+P_y^4+P_z^4) + \alpha_{12}(P_x^2P_y^2+P_x^2P_z^2+P_y^2P_z^2)+K_{strain}(\mathbf{P}.\mathbf{u})^2 - \mathbf{P}.(\mathbf{F}_{ext}+\mathbf{F}_{DMI}), \quad (5)$$

where α_1, α_{11}, and α_{12} are the phenomenological Landau expansion coefficients, K_{strain} is the strain energy, $\mathbf{u}$ is the axis of substrate strain, $\mathbf{F}_{ext}$ is the external electric field, and $\mathbf{F}_{DMI}$ is the effective electric field from DMI, which is discussed below. The strain term, $K_{strain}(\mathbf{P}.\mathbf{u})^2$, in Eq. (5) arises from the substrate-induced strain,[37,38] which dictates the energy-favorable planes for the equilibrium states of $\mathbf{P}$, thereby reducing the degeneracy of $\mathbf{P}$ orientations in the specific case of the MF $BiFeO_3$, which is shown in previous studies.[14,39,40]

In the model presented in this study, we take a highly simplified mathematical approach to phenomenologically count for the complex interactions between the FM and MF layers. We merge the exchange coupling, which couples $\mathbf{M}_C$ in $BiFeO_3$ and $\mathbf{M}$ in CoFe, and the DMI, which couples $\mathbf{P}$ and $\mathbf{M}_C$ in $BiFeO_3$, into one effective DMI term that directly captures the interaction between $\mathbf{M}$ in CoFe and $\mathbf{P}$ in $BiFeO_3$, with an effective Hamiltonian,[14,27]

$$E_{DMI} = -E_{DMI,0}\hat{\mathbf{P}}.(\hat{\mathbf{N}}\times\hat{\mathbf{M}}), \quad (6)$$

where $E_{DMI,0}$ is the energy coefficient of DMI, $\hat{\mathbf{P}}$ is the polarization of $BiFeO_3$, $\hat{\mathbf{N}}$ is the Neel vector, and $\hat{\mathbf{M}}$ is the magnetic moment in CoFe. All vectors in the equation are normalized vectors. The effective magnetic field ($\mathbf{H}_{DMI}$) and electric field ($\mathbf{F}_{DMI}$) that enter the equations of motions are then

$$\mathbf{H}_{DMI} = -\frac{1}{\mu_0 M_S}\frac{\partial E_{DMI}}{\partial \hat{\mathbf{M}}} \equiv H_{DMI,0}(\hat{\mathbf{P}}\times\hat{\mathbf{N}}) \quad (7)$$

and

$$\mathbf{F}_{DMI} = -\frac{1}{P_S}\frac{\partial E_{DMI}}{\partial \hat{\mathbf{P}}} \equiv F_{DMI,0}(\hat{\mathbf{N}}\times\hat{\mathbf{M}}), \quad (8)$$

where $H_{DMI,0}$ is the effective DMI magnetic field magnitude and $F_{DMI,0}$ is the effective DMI electric field magnitude. Both fields are assumed to have constant magnitudes for specific material combinations because they originate from the energy and material parameters,

$$E_{DMI,0} = \mu_0 M_S.H_{DMI,0} = P_S.F_{DMI,0}. \quad (9)$$

With the direction of $\mathbf{N}$ defined as $\hat{\mathbf{N}} = -\hat{\mathbf{P}}\times\hat{\mathbf{M}}$, all vectors in the CoFe/$BiFeO_3$ FM/MF system ($\mathbf{P}$, $\mathbf{N}$, and $\mathbf{M}$) are connected by the DMI. The method of implementing the dynamic evolution of $\mathbf{M}$ and $\mathbf{P}$ described above is shown schematically in Fig. 2. The initial state of the SOTFET is defined by a set of vectors: $\mathbf{M}$ in the FM and $\mathbf{M}_C$, $\mathbf{P}$, and $\mathbf{N}$ in the MF layer. When a current J_{SO} flows in the SO layer, all four vectors ($\mathbf{M}$, $\mathbf{M}_C$, $\mathbf{P}$, and $\mathbf{N}$) can switch to different states, with dynamics dictated by the LLGS and the LK equations in each loop. Finally, a set of four vectors in a different equilibrium state will be reached by iteration. The switching behavior of $\mathbf{P}$ and $\mathbf{M}$ is assumed to be purely rotational, consistent with experimental studies of $BiFeO_3$.[14]

Key parameters used in the numerical evaluation of the SOTFET are provided in supplementary material S1. The model is validated by comparing with the micromagnetic simulation tools OOMMF[41] and MuMax3[42] and other theoretical calculations and experimental results, shown in supplementary material S2. For the SOTFET gate stack to controllably gate the semiconductor channel, a deterministic switching of polarization $\mathbf{P}$ in the z-direction in the MF layer is desired.

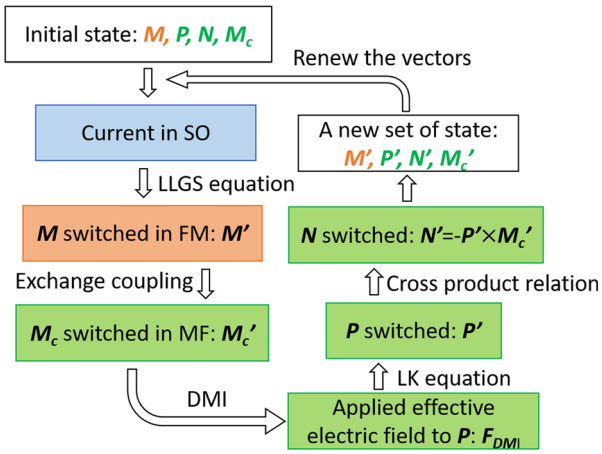

FIG. 2. Computation flow chart of the SOTFET modeling procedure.

For the CoFe/$BiFeO_3$ FM/MF heterostructure and taking $P_S = 100\ \mu C/cm^2$ of $BiFeO_3$[43] and $M_S = 1.6\times10^6$ A/m of CoFe,[15] switching behavior for a range of assumed DMI energies is shown in Fig. 3(a). Upon applying a current of $J_{SO} = -30$ MA/cm^2, different switching behavior of the $x-$ component of the magnetization (M_x) is observed for different DMI energies. For these values, however, the $z-$ component of polarization P_z in the MF layer does *not* follow the motions of $\mathbf{M}$. This is because, given the large P_S, a moderate DMI energy is not sufficient to overcome the anisotropy energy in $\mathbf{P}$ to switch it. For a high DMI energy, with $\mathbf{P}$ held in place, $\mathbf{M}$ also does not switch because H_{DMI} then functions as an effective unidirectional anisotropy acting back on $\mathbf{M}$. This is, therefore, a situation when the SOTFET does not achieve the desired functionality.

The natural next step is to explore reduced P_S in the MF layer. Reducing P_S in $BiFeO_3$ is experimentally feasible, for example, by La substitution of Bi in $BiFeO_3$.[44,45] Recent experiments by Lin *et al.*[46] also show that the exchange interaction between CoFe and La-substituted $BiFeO_3$ remains strong even with reduced P_S. Qualitatively, this implies that the multiferroic layer should have a relatively weak ferroelectricity, a strong magnetization, and strong coupling between the two order parameters. The calculated results with a reduced $P_S = 10\ \mu C/cm^2$ and other parameters unchanged are shown in Fig. 3(b) for a range of $E_{DMI,0}$ values. For the same current J_{SO}, a critical $E_{DMI,0}$ is observed. Above the critical $E_{DMI,0}$, M_x and P_z concomitantly switch, signaling the required materials parameters for desired SOTFET operation.

Reducing P_S of the multiferroic could help the switching of $\mathbf{P}$ for two reasons. First, as shown in Eq. (9), for a fixed $H_{DMI,0}$ and M_S, lowering P_S for the same $E_{DMI,0}$ implies an enhanced $F_{DMI,0}$ to switch the polarization. Second, a reduced P_S leads to a weaker polarization anisotropy as described in the free energy equation, Eq. (5). This lowers the energy barrier between polarization equilibrium states, making the switching easier.

Figures 3(c) and 3(d) show that the desired stable switching behavior of the SOTFET is achieved by choosing the CoFe/$BiFeO_3$ heterostructure with a reduced $P_S = 10\ \mu C/cm^2$ of the MF layer

Published under license by AIP Publishing

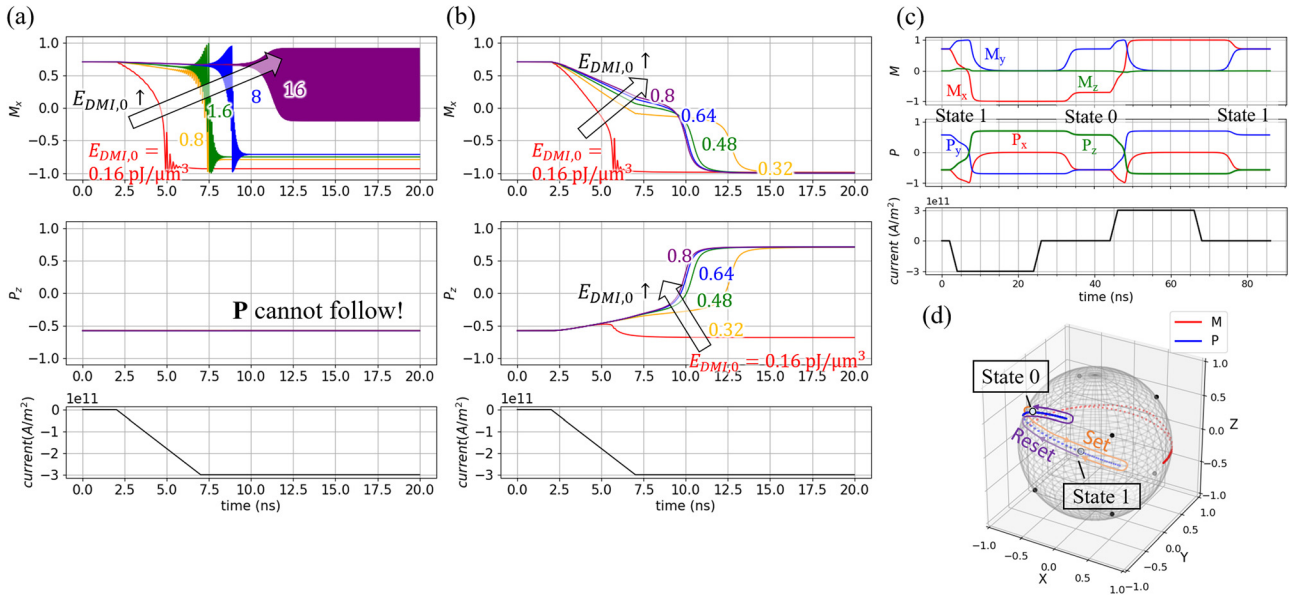

FIG. 3. Switching behavior in a SOTFET gate stack for a range of assumed DMI energies assuming (a) $P_S = 100\ \mu C/cm^2$ and (b) $P_S = 10\ \mu C/cm^2$. For a high P_S in (a), it is observed that upon applying a current J_{SO} (lower panel), M_x responds to the spin–orbit torque (upper panel); P_z, however, does not switch (mid-panel). For a lower P_S in (b), it is observed that above a critical DMI energy, both M_x and P_z switch deterministically. (c) and (d) **M** and **P** can be switched by J_{SO} into 0 and 1 states while showing non-volatility; $P_S = 10\ \mu C/cm^2$ and $E_{DMI,0} = 0.8\ pJ/\mu m^3$ are assumed. (d) shows the trajectories of **M** (red) and **P** (blue) on a sphere. The set to 1 (**P** = [−1, 1, −1]) process is marked by orange and the reset to 0 (**P** = [−1, −1, 1]) by purple.

($BiFeO_3$) and an above-critical $E_{DMI,0} = 0.8\ pJ/\mu m^3$, which corresponds to DMI fields of $H_{DMI,0} = 5$ kOe and $F_{DMI,0} = 80$ kV/cm. It is seen that switching the current direction in the SO layer switches P_z. The current density used, 30 MA/cm^2, is about one order of magnitude lower than that of heavy metal-based SOT-MRAMs[47,48] due to the assumed large spin Hall angle of Bi_2Se_3 ($\theta_{AD} = \theta_{FL} = 3.5$[23]) and can be further reduced by using larger spin Hall angle materials such as BiSb.[49] The current necessary to switch a SOTFET is still rather high, which partly stems from the coupling between the MF and FM layers, which increases the energy barrier to switch **M** by current. More discussions on the dependence of the critical current on the DMI energy can be found in supplementary material S3. With a suitable current applied, **M** is observed to switch within the x–y plane and **P** is switched out-of-plane. The switching trajectories of **M** and **P** are shown in the spherical plot in Fig. 3(d). Clear set and reset processes between State 0 and 1 are observed, proving the feasibility of the SOTFET operation for the chosen material parameters.

The switching of **P** with a reduced $P_S = 10\ \mu C/cm^2$ shown in Figs. 3(c) and 3(d) results in a charge difference of $\Delta Q = 2P_z \approx 12\ \mu C/cm^2$ in the semiconductor channel, assuming the absence of traps at the interface between the MF layer and the semiconductor channel. For example, for the choice of a silicon channel, this will lead to a surface potential change approximately at $\Delta\psi \approx 1.3$ V by a simple calculation,[50] accessing the entire operating regime of a MOSFET from strong inversion to accumulation. Thus, by estimation, at least an on/off ratio of 10^8 in I_D can be achieved due to the resistance change of the channel, which, in practice, will be limited by gate leakage and interfacial trap states rather than the intrinsic capability of a SOTFET. The simulation integrated with a Si-MOSFET model in SPICE verifies that an on/off ratio $>10^7$ can be achieved,[16] which indicates that a $P_S \approx 0.1\ \mu C/cm^2$ is sufficient to fully control the semiconductor channel for the high on/off ratio when assuming no defect. The high on/off ratio in I_D as the readout component brings the read energy of a SOTFET down to the same level as a conventional semiconductor transistor. As a result, the write energy for a SOTFET should be comparable to that of a SOT MRAM, while the read energy is comparable to that of a FeFET; these features, together with the logic functionalities discussed later, make SOTFET a potentially competitive technology.

An electrically insulating magnetic (FM) layer is more desirable for SOTFET application in order to reduce the shunting current from the SO layer and boost the spin torque efficiency.[51] Besides, the insulating FM layer could reduce the charge injection in the MF layer, thus potentially alleviating the fatigue that is often confronted by ferroelectric materials. The fatigue issue could also be addressed by the fact that the polarization switching is driven by coupling to the magnetic layer rather than an external electric field, which could reduce the tendency for long-distance atom motion.

Another challenge in the development of ferroelectric memory devices has been the presence of the depolarization field that can destabilize the ferroelectric polarization over time.[52] If the hierarchy of coupling energies within the SOTFET is designed correctly, **P** cannot switch unless **M** is switched by J_{SO}. We envision that, as a result, the exchange coupling of the multiferroic to the magnetic layer could improve the ferroelectric retention.

In addition, by the virtue of simultaneously being a FET, the SOTFET can also provide logic functionality by a gate voltage controlling the channel. As a merger of memory and logic, the SOTFET is capable of performing process-in-memory (PiM) functionalities that significantly lower the energy consumption and physical size of

Published under license by AIP Publishing

computation, compared to a von Neumann architecture where logic and memory are separated. Some examples are explored in Ref. 16. The experimental realization and various modes of operation of the SOTFET are currently being investigated.

In summary, the SOTFET, a magnetoelectric memory device, is proposed, in which a change in magnetization of a SO/FM layer is transduced to control the semiconductor channel by using a magnetoelectric multiferroic layer, so that a read out with several orders of magnitude change in resistance can be achieved. We establish a quantitative model of the dynamics of the magnetization and polarization of the layers of the SOTFET. From the model, the material needs for the desired operation are identified and the feasibility of the SOTFET is proved in a properly designed CoFe/$BiFeO_3$ gate stack.

See the supplementary material for the key parameters for numerical simulations, validation of the model, and discussions on the dependence of the critical current on the DMI energy.

This work was supported in part by the Semiconductor Research Corporation (SRC) as nCORE task 2758.001 and NSF under the E2CDA program (No. ECCS 1740286). The authors wish to thank Professor Alyosha Molnar, Professor Christopher Batten, Yu-Ching Liao, Hyunjea Lee, and Yongjian (Helffor) Tang for helpful discussions.

REFERENCES

[1]F. Hellman, A. Hoffmann, Y. Tserkovnyak, G. S. D. Beach, E. E. Fullerton, C. Leighton, A. H. MacDonald, D. C. Ralph, D. A. Arena, H. A. Durr, P. Fischer, J. Grollier, J. P. Heremans, T. Jungwirth, A. V. Kimel, B. Koopmans, I. N. Krivorotov, S. J. May, A. K. Petford-Long, J. M. Rondinelli, N. Samarth, I. K. Schuller, A. N. Slavin, M. D. Stiles, O. Tchernyshyov, A. Thiaville, and B. L. Zink, Rev. Mod. Phys. **89**, 025006 (2017).
[2]M. N. Baibich, J. M. Broto, A. Fert, F. N. Van Dau, F. Petroff, P. Etienne, G. Creuzet, A. Friederich, and J. Chazelas, Phys. Rev. Lett. **61**, 2472–2475 (1988).
[3]A. Fert, Rev. Mod. Phys. **80**, 1517 (2008).
[4]P. A. Grunberg, Rev. Mod. Phys. **80**, 1531 (2008).
[5]J. C. Slonczewski, Phys. Rev. B **39**, 6995 (1989).
[6]J. C. Slonczewski, J. Magn. Magn. Mater. **159**, L1–L7 (1996).
[7]L. Berger, Phys. Rev. B **54**, 9353 (1996).
[8]D. C. Ralph and M. D. Stiles, J. Magn. Magn. Mater. **320**, 1190–1216 (2008).
[9]I. M. Miron, K. Garello, G. Gaudin, P.-J. Zermatten, M. V. Costache, S. Auffret, S. Bandiera, B. Rodmacq, A. Schuhl, and P. Gambardella, Nature **476**, 189–193 (2011).
[10]L. Liu, C.-F. Pai, Y. Li, H. W. Tseng, D. C. Ralph, and R. A. Buhrman, Science **336**, 555–558 (2012).
[11]R. Ramesh and N. A. Spaldin, Nat. Mater. **6**, 21–29 (2007).
[12]M. Fiebig, T. Lottermoser, D. Meier, and M. Trassin, Nat. Rev. Mater. **1**, 16046 (2016).
[13]Y.-H. Chu, L. W. Martin, M. B. Holcomb, and R. Ramesh, Mater. Today **10**, 16–23 (2007).
[14]J. T. Heron, J. L. Bosse, Q. He, Y. Gao, M. Trassin, L. Ye, J. D. Clarkson, C. Wang, J. Liu, S. Salahuddin, D. C. Ralph, D. G. Schlom, J. Iniguez, B. D. Huey, and R. Ramesh, Nature **516**, 370–373 (2014).
[15]D. Y. Qiu, K. Ashraf, and S. Salahuddin, Appl. Phys. Lett. **102**, 112902 (2013).
[16]O. Afuye, X. Li, F. Guo, D. Jena, D. C. Ralph, A. Molnar, H. G. Xing, and A. Apsel, IEEE J. Explor. Solid-State Comput. Devices Circuits **5**, 197 (2019).
[17]M. I. Dyakonov and V. I. Perel, Phys. Lett. A **35**, 459–460 (1971).
[18]J. E. Hirsch, Phys. Rev. Lett. **83**, 1834 (1999).
[19]J. Sinova, S. O. Valenzuela, J. Wunderlich, C. H. Back, and T. Jungwirth, Rev. Mod. Phys. **87**, 1213 (2015).
[20]Y. A. Bychkov, E. I. R. Y. A. Bychkov, and E. I. Rashba, J. Phys. C **17**, 6039 (1984).
[21]L. Fu and C. L. Kane, Phys. Rev. B **76**, 045302 (2007).
[22]M. Z. Hasan and C. L. Kane, Rev. Mod. Phys. **82**, 3045 (2010).
[23]A. R. Mellnik, J. S. Lee, A. Richardella, J. L. Grab, P. J. Mintun, M. H. Fischer, A. Vaezi, A. Manchon, E.-A. Kim, N. Samarth, and D. C. Ralph, Nature **511**, 449–451 (2014).
[24]I. Dzyaloshinsky, J. Phys. Chem. Solids **4**, 241–255 (1958).
[25]T. Moriya, Phys. Rev. **120**, 91–98 (1960).
[26]J. T. Heron, M. Trassin, K. Ashraf, M. Gajek, Q. He, S. Y. Yang, D. E. Nikonov, Y.-H. Chu, S. Salahuddin, and R. Ramesh, Phys. Rev. Lett. **107**, 217202 (2011).
[27]C. Ederer and N. A. Spaldin, Phys. Rev. B **71**, 060401(R) (2005).
[28]S. George, K. Ma, A. Aziz, X. Li, A. Khan, S. Salahuddin, M. Chang, S. Datta, J. Sampson, S. Gupta, and V. Narayanan, "Nonvolatile memory design based on ferroelectric FETs," in 2016 53rd ACM/EDAC/IEEE Design Automation Conference (DAC) (2016), pp. 1–6.
[29]J. F. Scott and C. A. P. de Araujo, Science **246**, 1400–1405 (1989).
[30]S. L. Miller and P. J. McWhorter, J. Appl. Phys. **72**, 5999 (1992).
[31]S. Salahuddin and S. Datta, Nano Lett. **8**(2), 405 (2008).
[32]P. Dang, Z. Zhang, J. Casamento, X. Li, J. Singhal, D. G. Schlom, D. C. Ralph, H. G. Xing, and D. Jena, IEEE J. Explor. Solid-State Comput. Devices Circuits **5**, 158–165 (2019).
[33]J. Xiao, A. Zangwill, and M. D. Stiles, Phys. Rev. B **72**, 014446 (2005).
[34]S. Yan, Z. Sun, and Y. B. Bazaliy, Phys. Rev. B **88**, 054408 (2013).
[35]M. Beleggia, M. D. Graef, and Y. T. Millev, J. Phys. D **39**, 891–899 (2006).
[36]L. D. Landau and I. M. Khalatnikov, Dokl. Akad. Nauk SSSR **96**, 469–472 (1954).
[37]Y.-C. Liao, D. E. Nikonov, S. Dutta, S.-C. Chang, S. Manipatruni, I. A. Young, and A. Naeemi, arXiv:1902.03330 (2019).
[38]J. X. Zhang, Y. L. Li, Y. Wang, Z. K. Liu, L. Q. Chen, Y. H. Chu, F. Zavaliche, and R. Ramesh, J. Appl. Phys. **101**, 114105 (2007).
[39]J. Li, J. Wang, M. Wuttig, R. Ramesh, N. Wang, B. Ruette, A. P. Pyatakov, A. K. Zvezdin, and D. Viehland, Appl. Phys. Lett. **84**, 5261 (2004).
[40]A. B. Mei, Y. Tang, J. Schubert, D. Jena, H. G. Xing, D. C. Ralph, and D. G. Schlom, APL Mater. **7**, 071101 (2019).
[41]M. J. Donahue and D. G. Porter, "OOMMF user's guide, version 1.0," Interagency Report No. NISTIR 6376 (National Institute of Standards and Technology, Gaithersburg, MD, 1999).
[42]A. Vansteenkiste, J. Leliaert, M. Dvornik, M. Helsen, F. Garcia-Sanchez, and B. V. Waeyenberge, AIP Adv. **4**, 107133 (2014).
[43]J. Wang, J. B. Neaton, H. Zheng, V. Nagarajan, S. B. Ogale, B. Liu, D. Viehland, V. Vaithyanathan, D. G. Schlom, U. V. Waghmare, N. A. Spaldin, K. M. Rabe, M. Wuttig, and R. Ramesh, Science **299**, 1719–1722 (2003).
[44]S. K. Singh and H. Ishiwara, Jpn. J. Appl. Phys., Part 1 **45**, 3194 (2006).
[45]O. E. Gonzalez-Vazquez, J. C. Wojdel, O. Dieguez, and J. Iniguez, Phys. Rev. B **85**, 064119 (2012).
[46]C.-C. Lin, T. Gosavi, D. Nikonov, Y.-L. Huang, B. Prasad, W. Choi, V. T. Pham, I. Groen, J.-Y. Chen, M. DC, H. Liu, K. Oguz, E. S. Walker, J. Plombon, B. Buford, C. H. Naylor, J.-P. Wang, F. Casanova, R. Ramesh, and I. A. Young, in 2019 IEEE International Electron Device Meeting (IEDM), San Francisco, CA (2019), pp. 37.3.1–37.3.4.
[47]K. Meng, J. Miao, X. Xu, Y. Wu, J. Xiao, J. Zhao, and Y. Jiang, Sci. Rep. **6**, 38375 (2016).
[48]K. K. Meng, J. Miao, X. G. Xu, Y. Wu, X. P. Zhao, J. H. Zhao, and Y. Jiang, Phys. Rev. B **94**, 214413 (2016).
[49]N. H. D. Khang, Y. Ueda, and P. N. Hai, Nat. Mater. **17**, 808–813 (2018).
[50]T. Ytterdal, Y. Cheng, and T. A. Fjeldly, *Device Modeling for Analog and RF CMOS Circuit Design* (John Wiley and Sons, Ltd., 2003).
[51]H. Wang, J. Kally, J. S. Lee, T. Liu, H. Chang, D. R. Hickey, K. A. Mkhoyan, M. Wu, A. Richardella, and N. Samarth, Phys. Rev. Lett. **117**, 076601 (2016).
[52]R. R. Mehta, B. D. Silverman, and J. T. Jacobs, J. Appl. Phys. **44**, 3379 (1973).

Published under license by AIP Publishing

Spin-Orbit Torque Field-Effect Transistor (SOTFET): Proposal for a Magnetoelectric Memory Supplementary Materials

Xiang Li,[1, a)] Joseph Casamento,[2] Phillip Dang,[3] Zexuan Zhang,[1] Olalekan Afuye,[1] Antonio B. Mei,[2] Alyssa B. Apsel,[1] Darrell G. Schlom,[2] Debdeep Jena,[1, 2, 4] Daniel C. Ralph,[4, 5] and Huili Grace Xing[1, 2, 4]

[1)] *School of Electrical and Computer Engineering, Cornell University, Ithaca, NY 14853, USA.*

[2)] *Department of Materials Science and Engineering, Cornell University, Ithaca, NY 14853, USA.*

[3)] *School of Applied and Engineering Physics, Cornell University, Ithaca, NY 14853, USA.*

[4)] *Kavli Institute at Cornell for Nanoscale Science, Ithaca, NY 14853, USA.*

[5)] *Department of Physics, Cornell University, Ithaca, NY 14853, USA.*

(Dated: 23 April 2020)

S1. KEY PARAMETERS IN THE MODEL

Key parameters used in the LLGS equation to describe **M** dynamics are listed in Table S1. The spin Hall angle of Bi_2Se_3 is assumed and other material parameters of CoFe are used in the LLGS equation.

TABLE S1. Parameters used in the LLGS equation

Parameter	Symbol	Value	Unit
Spin Hall angle	$\theta_{AD(FL)}$	3.5 [1]	-
Electron gyromagnetic ratio	γ	1.76×10^{11}	$s^{-1}T^{-1}$
Gilbert damping factor	α	0.01 [2]	-
Saturation magnetization	M_S	1.6×10^{6} [3]	A/m
Anisotropy constant	K	1.5×10^{4} [4]	J/m^3
External field	H_{ext}	0	A/m
Ferromagnetic thickness	t	3	nm
Device length/width	L_x/L_y	30	nm

Key parameters used in the LK equation to describe **P** dynamics are shown in Table S2. The material parameters of $BiFeO_3$ are used in the LK equation.

TABLE S2. Parameters used in the LK equation

Parameter	Symbol	Value	Unit
Viscosity coefficient	γ_{FE}	5×10^{-3} [5]	m·s/F
Landau coefficients	α_1	-4×10^{8} [6]	$C^{-2}m^2N$
	α_{11}	6.5×10^{8} [6]	$C^{-4}m^6N$
	α_{12}	1×10^{8} [6]	$C^{-4}m^6N$
Strain energy	K_{strain}	6×10^{6}	J/m^3
Strain axis	**u**	[0, 1, 1]	-

S2. VALIDATION OF THE MODEL

For the magnetic dynamics described by the LLGS equation, comparisons with existing magnetic simulation tools such as OOMMF[7] and MuMax3[8] are used to validate the model developed in this work. The responses of the ferromagnetic layer to spin-orbit torques that we calculate match well with the results from OOMMF and MuMax3, as shown by selected results in Fig. S1(a). Our results also agree with switching behavior calculated analytically[9].

For the ferroelectric dynamics described by the LK equation, we performed test simulations as a function of applied electric field for the $BiFeO_3$ material system. With the inclusion of a depolarization term to model the effect of domain walls[5], we find two-step **P** switching in agreement with previous theoretical and experimental works in[10], with the trajectory of **P** switching shown in Fig. S1(b).

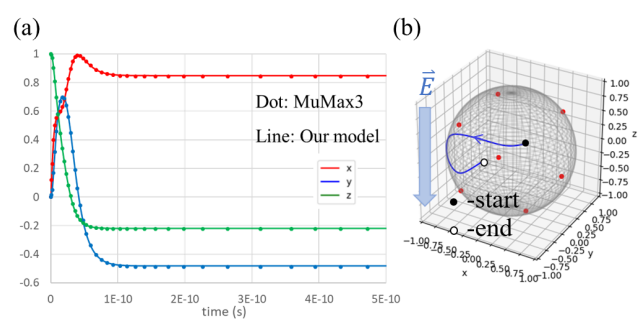

FIG. S1. Validation of the SOTFET model. (a) The *xyz* components versus time plot when **M** of FM is switched by spin-orbit torque from the SO layer. Results from MuMax3 are shown by the dots and results from this model are shown by the line. (b) A two-step switching trajectory of **P** in $BiFeO_3$ with an applied electric field in the $-z$ direction. Red dots represent the 8 stable states of **P**.

[a)] Electronic mail: xl633@cornell.edu

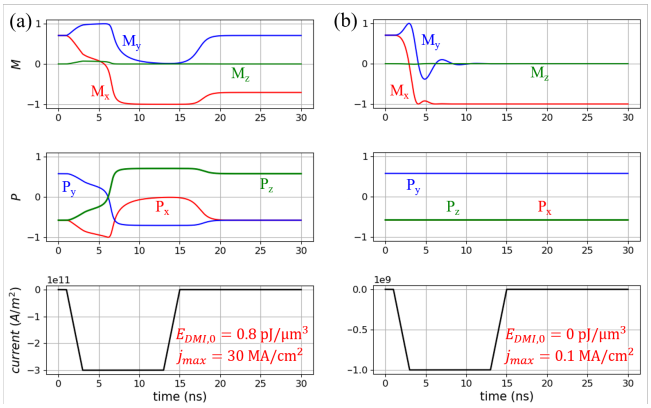

FIG. S2. SOTFET behavior where the FM layer is switched at a critical current J_{SO} with (a) $E_{DMI,0}$=0.8 pJ/μm^3 (strong coupling between **M** and **P** thus switching of **M** resulting in switching of **P**) and (b) $E_{DMI,0}$=0 pJ/μm^3 (**M** and **P** decoupled thus no switching in **P** though **M** is switched). With the strong coupling between FM and MF layers, the critical current increases more than 2 orders of magnitude.

S3. CRITICAL CURRENT DEPENDENCE ON DMI ENERGY

The presence of exchange interaction and DMI between FM and MF will result in a higher critical current to switch the magnetization in the FM layer, comparing to the case when FM and MF are decoupled. In Fig. S2, we show the critical switching cases with different effective DMI energies ($E_{DMI,0}$). With strong coupling presented between **M** and **P** (high $E_{DMI,0}$, Fig. S2(a)), the critical current of switching in-plane magnetization is more than 2 orders magnitude higher than the decoupled case ($E_{DMI,0}$=0, Fig. S2(b)). This indicates that the presence of exchange coupling and DMI increases the energy barrier to switch **M**, thus leading to a significant increase in the critical current.

[1] A. R. Mellnik, J. S. Lee, A. Richardella, J. L. Grab, P. J. Mintun, M. H. Fischer, A. Vaezi, A. Manchon, E.-A. Kim, N. Samarth, and D. C. Ralph, Nature **511**, 449–451 (2014).
[2] Y. Henry, S. Mangin, J. Cucchiara, J. A. Katine, and E. E. Fullerton, Phys. Rev. B **79**, 214422 (2009).
[3] D. Y. Qiu, K. Ashraf, and S. Salahuddin, Appl. Phys. Lett. **102**, 112902 (2013).
[4] T. A. Moore, M. J. Walker, A. S. Middleton, and J. A. C. Bland, J. Appl. Phys. **97**, 053903 (2005).
[5] Y.-C. Liao, D. E. Nikonov, S. Dutta, S.-C. Chang, S. Manipatruni, I. A. Young, and A. Naeemi, arXiv:1902.03330 (2019).
[6] J. X. Zhang, Y. L. Li, Y. Wang, Z. K. Liu, L. Q. Chen, Y. H. Chu, F. Zavaliche, and R. Ramesh, J. Appl. Phys. **101**, 114105 (2007).
[7] M. J. Donahue and D. G. Porter, OOMMF User's Guide, Version 1.0, Interagency Report **NISTIR 6376**, National Institute of Standards and Technology, Gaithersburg, MD (1999).
[8] A. Vansteenkiste, J. Leliaert, M. Dvornik, M. Helsen, F. Garcia-Sanchez, and B. V. Waeyenberge, AIP Advances **4**, 107133 (2014).
[9] L. Liu, O. J. Lee, T. J. Gudmundsen, D. C. Ralph, and R. A. Buhrman, Phys. Rev. Lett. **109**, 096602 (2012).
[10] J. T. Heron, J. L. Bosse, Q. He, Y. Gao, M. Trassin, L. Ye, J. D. Clarkson, C. Wang, J. Liu, S. Salahuddin, D. C. Ralph, D. G. Schlom, J. Iniguez, B. D. Huey, and R. Ramesh, Nature **516**, 370–373 (2014).